Jaspine B induces nonapoptotic cell death in gastric cancer cells independently of its inhibition of ceramide synthase[s]

Francesca Cingolani,[1,2,]* Fabio Simbari,* Jose Luis Abad,* Mireia Casasampere,*
Gemma Fabrias,* Anthony H. Futerman,[†] and Josefina Casas[2,]*

Research Unit on BioActive Molecules (RUBAM), Department of Biomedicinal Chemistry,* Institute for Advanced Chemistry of Catalonia (IQAC-CSIC), Barcelona, Spain; and Department of Biological Chemistry,[†] Weizmann Institute of Science, Rehovot, Israel

Abstract Sphingolipids (SLs) have been extensively investigated in biomedical research due to their role as bioactive molecules in cells. Here, we describe the effect of a SL analog, jaspine B (JB), a cyclic anhydrophytosphingosine found in marine sponges, on the gastric cancer cell line, HGC-27. JB induced alterations in the sphingolipidome, mainly the accumulation of dihydrosphingosine, sphingosine, and their phosphorylated forms due to inhibition of ceramide synthases. Moreover, JB provoked atypical cell death in HGC-27 cells, characterized by the formation of cytoplasmic vacuoles in a time and dose-dependent manner. Vacuoles appeared to originate from macropinocytosis and triggered cytoplasmic disruption. The pan-caspase inhibitor, z-VAD, did not alter either cytotoxicity or vacuole formation, suggesting that JB activates a caspase-independent cell death mechanism. The autophagy inhibitor, wortmannin, did not decrease JB-stimulated LC3-II accumulation. In addition, cell vacuolation induced by JB was characterized by single-membrane vacuoles, which are different from double-membrane autophagosomes.[jlr] These findings suggest that JB-induced cell vacuolation is not related to autophagy and it is also independent of its action on SL metabolism.—Cingolani, F., F. Simbari, J. L. Abad, M. Casasampere, G. Fabrias, A. H. Futerman, and J. Casas. **Jaspine B induces nonapoptotic cell death in gastric cancer cells independently of its inhibition of ceramide synthase.** *J. Lipid Res.* 2017. **58:** 1500–1513.

Supplementary key words sphingolipid • liquid chromatography-mass spectrometry • methuosis • autophagy • anticancer drug

Sphingolipids (SLs) are both structural components of cell membranes and bioactive molecules (1). SL metabolism is a complex network of highly regulated reactions (2) and its alteration is related to a variety of diseases (3), including the sphingolipidoses (4), cancer (5), inflammation (6), and neurological disorders (7, 8). SLs are not only present in mammals, but also in prokaryotes and other eukaryotes (9). The structural and functional variety of these naturally occurring molecules represents a remarkable source of potential therapeutic agents. Natural SLs extracted from fungi and marine organisms display structural similarities to mammalian SLs and can interact with endogenous SL metabolism, and have therefore been investigated as therapeutic agents for the treatment of different diseases, including cancer (10).

The natural SL, jaspine B (JB) (**Fig. 1**), is a cyclic anhydrophytosphingosine isolated from the marine sponges, *Pachastissamine sp.* (11) and *Jaspis sp.* (12). JB is cytotoxic (11) and induces apoptotic and autophagy-mediated cell death in human and mouse cancer cell lines (13–14). These processes have been associated with alterations in SL metabolism. JB has been synthesized through various synthetic routes [(15, 16) and references therein]. Moreover, a series of JB derivatives have been prepared including triazole-JB hybrids (17) and carbocyclic JB (18) and aza-JB (19) analogs. In a previous report, we investigated the biological activity of diastereomeric JB, including JB with the natural configuration and three stereoisomers, namely 2,3-*epi* JB, 2-*epi* JB, and 3-*epi* JB (Fig. 1). JB was the most cytotoxic

---

Abbreviations: Cer, ceramide; CerS, ceramide synthase; dhCer, dihydroceramide; dhSo, dihydrosphingosine; dhSoP, dihydrosphingosine1-phosphate; EIPA, 5-(*N*-ethyl-*N*-isopropyl)amiloride; FB1, fumonisin B1; JB, jaspine B; LY, Lucifer Yellow; MTT, 3-(4,5-dimethylthiazol-2-yl)-2,5-diphenyl tetrazolium bromide; PB, phosphate buffer; PI, propidium iodide; SK, sphingosine kinase; SL, sphingolipid; So, sphingosine; SoP, sphingosine 1-phosphate; TEM, transmission electron microscopy.

[1] Present address of F. Cingolani: Division of Digestive Diseases, Department of Medicine, Emory University School of Medicine, Atlanta, GA.

[2] To whom correspondence should be addressed.
  e-mail: fina.casas@iqac.csic.es (J.C.); fcingol@emory.edu (F.C.)
[S] The online version of this article (available at http://www.jlr.org) contains a supplement.
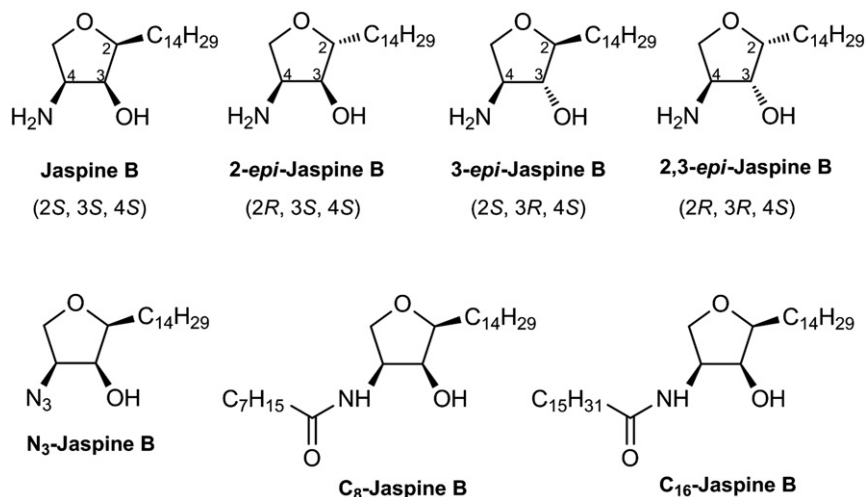
Fig. 1. Chemical structure of JB and analogs.

molecule in A549 cancer cells, whereas diastereomeric JBs were 10–20 times less toxic (14). In another study, these four molecules, together with their enantiomeric pairs, exhibited moderate to potent inhibition of sphingosine (So) kinase (SK)1 and SK2. Moreover atypical PKCs were inhibited by several JB stereoisomers (20).

Ceramide synthases (CerSs) are responsible for ceramide (Cer) and dihydroceramide (dhCer) synthesis by N-acylation of the sphingoid bases, So and dihydrosphingosine (dhSo), respectively (21). Each of the six mammalian CerSs (CerS1–6) catalyzes addition of a restricted subset of acyl-CoAs with different fatty acid chain lengths to the sphingoid long-chain base (22). Both sphingoid bases and their acylated counterparts have been shown to play essential roles in cell fate determination. Although Cer is the most typical inducer of cell growth arrest and apoptosis (23), similar functions have also been reported for So (24, 25) and dhSo (26, 27) in various cells. More recently, dhCer has also emerged as an active modulator of many cellular responses, including cell death (28, 29) and autophagy (30). Therefore, modulation of CerS activity might result in altered levels of bioactive SLs, representing an attractive target in biomedical research.

In this report, we investigate the effect of JB on SL metabolism and cell viability in the gastric cancer cell line, HGC-27. We show that JB inhibits CerS, which in turn leads to the accumulation of free sphingoid bases and alteration of the lipidome. Moreover, JB induces cell death through a non-apoptotic and nonautophagic mechanism in which HGC-27 cells engulf large amounts of extracellular fluid by macropinocytosis, leading to bulk vacuolation and death. Importantly the same vacuolation process also occurs in other cancer cell models, suggesting the generality of this effect.

MATERIALS AND METHODS

Synthesis of N-acyl JB by Staudinger ligation between N₃-JB and carboxylic acids

A solution of the corresponding carboxylic acid (0.10 mmol) in THF (1 ml) was treated with a solution of HOBt (14 mg, 0.09 mmol) and EDC (19 mg, 0.12 mmol) in THF (1 ml) under Ar. The resulting mixture was stirred for 15 min and then added dropwise over a solution of the starting azide (N₃-JB, 20 mg, 0.06 mmol in 1 ml THF) with triphenyl phosphine (27 mg, 0.1 mmol in 1 ml THF) for 15 min under Ar. The resulting solution was stirred at room temperature for 1 h and then quenched by addition of water (25 ml). The aqueous phase was extracted with DCM (3 × 10 ml) and the combined organic extracts were dried and evaporated to dryness to give a residue, which was chromatographed on a DCM-methanol gradient (0–4%) to give the corresponding amides as waxy solids.

N-octanoyl JB. $R_f = 0.45$ (DCM-methanol 9:1). ^{1}HNMR (400 MHz, CDCl$_3$): δ 6.15 (broad d, 1H, amide), 4.55 (m, 1H), 4.07 (m. 2H), 3.74 (m, 1H), 3.54 (app t, 1H), 2.18 (t, 2H), 1.60 (broad, 4H), 1.24 (broad, 32H), 0.85 (t, 2 × 3H). HRMS, calculated for C$_{26}$H$_{51}$NO$_3$ (M + 1): 426.3947; found: 426.3968.

N-palmitoyl JB. $R_f = 0.50$ (DCM-methanol 9:1). ^{1}HNMR (400 MHz, CDCl$_3$): δ 6.20 (broad d, 1H, amide), 4.50 (m, 1H), 4.15 (m. 2H), 3.72 (m, 1H), 3.51 (m, 1H), 2.23 (t, 2H), 1.55 (broad, 4H), 1.26 (broad, 48H), 0.80 (t, 2 × 3H). HRMS, calculated for C$_{34}$H$_{67}$NO$_3$ (M + 1): 538.5199; found: 538.5207.

Reagents and antibodies

MEM, DMEM, FBS, nonessential amino acids, penicillin/streptomycin, trypsin-EDTA, polyethylenimine, 3-(4,5-dimethylthiazol-2-yl)-2,5-diphenyl tetrazolium bromide (MTT), BSA, protease inhibitors (aprotinin, leupeptin, and PMSF), fumonisin B1 (FB1), 5-(N-ethyl-N-isopropyl)amiloride (EIPA), GenElute™ mammalian genomic DNA miniprep kit, and HEPES buffer were from Sigma-Aldrich. z-VAD and bafilomycin-A were from Enzo Life Sciences. Annexin V-FITC early apoptosis detection kit was from Cell Signaling. Laemmli buffer and acrylamide were from Bio-Rad (Hercules, CA). DMEM FluoroBrite and the MicroBCA protein assay kit were from Thermo Scientific. SYBR® Safe DNA gel stain and Lucifer Yellow (LY) were from Life Technologies. Lysotracker Red DND-99 was from Invitrogen. Internal standards for lipidomics and NBD-sphinganine were from Avanti Polar Lipids. C16-[1-^{14}C]acyl-CoA was from American Radiolabeled Chemicals. Glass-bottom dishes were from MaTek Corporation. Methanol (gradient grade for LC), water for chromatography, and silica gel 60 TLC plates were from Merck (Darmstadt, Germany). Antibodies: LC3-II (rabbit) and p62 (mouse) were from Abcam; PARP (rabbit) was from Cell Signaling; and β-actin (mouse) was from Sigma. HRP-secondary antibodies and ECL were from GE Healthcare.

Cell lines

HGC-27 cells (human gastric cancer cells, provided by Prof. Riccardo Ghidoni, University of Milan, Italy) were maintained in MEM supplemented with 10% FBS, 1% nonessential amino acids, 100 IU/ml penicillin, and 100 µg/ml streptomycin. Cells were grown without reaching confluence. MDA-MB 231 and MDA-MB 468 (human breast cancer cells, provided by Dr. Timothy Thomson, Molecular Biology Institute of Barcelona, CSIC, Spain), T98 and U87 (human glioblastoma cells, provided by Dr. Guillermo Velasco, Complutense University of Madrid, Spain), and HEK293T (human embryonic kidney cells, purchased from ATCC) were cultured in DMEM supplemented with 10% FBS, 100 IU/ml penicillin, and 100 µg/ml streptomycin. All cells were maintained at 37°C in 5% CO_2.

Cell viability

Cells ($0.1–0.25 \times 10^6$/ml) were seeded in 96-well plates (0.1 ml/well) and grown for 24 h. Cell viability was examined in triplicate samples by MTT method after treatment with the indicated compounds or with the corresponding percentage of vehicle ($\leq 0.25\%$ ethanol).

Cell transfection

HEK293T cells were grown in 10 cm dishes until 60–70% confluency. Human CerS genes were cloned in pCMV-Tag2B vector with an N-terminal FLAG tag, or in pcDNA3 vector containing a HA tag (22). The transfection mix was prepared by adding 6 µg of plasmid and 15 µl of polyethylenimine to a final volume of 1,375 µl of DMEM, without FBS and antibiotics, per well. After mixing, the transfection mix was incubated for 20 min at room temperature. Cells were washed twice, medium was replaced with 8 ml of incomplete DMEM, and the transfection mix was added. After incubating cells for 5–6 h, 5 ml of DMEM complemented with FBS and antibiotics were added. Cells were collected by trypsinization after 36–48 h. Ectopic protein expression was evaluated by Western blot analysis.

Lipid analysis

Cells were seeded at 0.2×10^6 cells/ml in a 6-well plate (1 ml/well). After 24 h, medium was replaced with fresh medium containing either the treatment of interest or the corresponding vehicle as a control. After the indicated time of incubation, the medium was removed and cells were washed with PBS. Cells were collected by adding 400 µl of trypsin and 600 µl of medium; residuals cells were collected by further washing each well with 400 µl of medium. Ten microliters of the cell suspension were used to count cells for each sample. SL extracts with internal standards [N-dodecanoylsphingosine, N-dodecanoylglucosylsphingosine, N-dodecanoylsphingosylphosphorylcholine, C17-phinganine (0.2 nmol each), and C17-sphinganine-1-phosphate (0.1 nmol)] were prepared and analyzed as reported by UPLC-TOFMS or HPLC-MS/MS (31).

Phase contrast microscopy

Phase contrast pictures were taken using a Nikon Eclipse TS100 inverted microscope with a 40× objective connected to a Digital Sight DS-2Mv camera and acquired with Nis Element F 3.0 software.

Transmission electron microscopy

Cells were seeded at 10^5 cells/ml in 6-well plates and grown overnight. Medium was replaced with fresh medium containing JB (5 µM), XM462 (8 µM), or ethanol (0.14%). After 16 h of treatment, cells were collected with 400 µl trypsin-EDTA and 600 µl MEM and the pellet was washed twice with 1% PBS. Cells were fixed in fixing buffer [2% paraformaldehyde and 2.5% glutaraldehyde in 0.1 M phosphate buffer (PB) (pH 7.4)] for 30 min at 4°C. Samples were centrifuged (1 min, 200 g) and resuspended in the same fixation buffer overnight. After washing with PB, cells were treated with 1% OsO_4 and 0.8% $K_3[Fe(CN)_6]$ in 0.1 M PB. Cells were then dehydrated through an ethanol series (90, 96, and 100%). Cells were embedded in Spurr resin by polymerization at 60°C for 48 h. Ultrathin sections were obtained with ULTRACUT ultramicrotome and examined with a JEOL 1010 transmission electron microscope connected to a CCD Orius camera (Gatan) and acquired with Digital Micrograph software (Gatan). Cell fixation and analysis were carried out in collaboration with Scientific and Technological Centers, University of Barcelona.

CerS activity

HEK293T cells overexpressing CerS were homogenized in 20 mM HEPES-KOH (pH 7.2), 25 mM KCl, 250 mM sucrose, and 2 mM $MgCl_2$ containing a protease inhibitor cocktail (Sigma-Aldrich). Protein content was determined using the Bradford reagent (Bio-Rad). The assay was carried out as reported (22, 32). Cell homogenates were incubated at 37°C with 15 µM NBD-sphinganine, 20 µM defatted BSA, and 50 µM acyl-CoA in a 20 µl reaction volume. N-acylation was determined by incubating cell homogenates (1 µg) with 15 µM dhSo (or JB), 20 µM defatted BSA, and 0.01 µCi C16-[1-^{14}C]acyl-CoA/46 µM C16 acyl-CoA in a final volume of 250 µl. Reactions were terminated by the addition of 750 µl of chloroform-methanol (1:2, v/v), and lipids were extracted by adding 500 µl of chloroform and 750 µl of deuterium-depleted water. After centrifugation (1,000 g, 10 min), the water phase was removed. Lipids in the organic phase were then dried under N_2, resuspended in 110 µl chloroform-methanol (9:1, v/v), and separated by TLC using chloroform-methanol-2 M NH_4OH (40:10:1, v/v/v) as the developing solvent. NBD-labeled lipids were visualized using a Typhoon 9410 variable mode imager and quantified by ImageQuantTL (GE Healthcare, Chalfont St. Giles, UK). Radioactively labeled SLs were visualized using a phosphorimaging screen (Fuji, Tokyo, Japan), recovered from TLC plates by scraping the silica directly into scintillation vials, and quantified by liquid scintillation counting.

Annexin V-FITC staining

Cells were plated at 10^5 cells/ml in 6-well plates and grown overnight. After treatment, cells, together with the medium, were collected with trypsin-EDTA and 1% BSA. Samples were centrifuged and pellets washed with 50 mM PBS-EDTA and 1% BSA. For cell staining, an Annexin V-FITC kit was used according to the manufacturer's instructions. Stained cells were analyzed by using a Guava EasyCyte™ flow cytometer (Merck Millipore, Billerica, MA). Data analysis was performed using the Multicycle AV program (Phoenix Flow Systems, San Diego, CA).

Western blotting

HGC-27 cells (10^5 cells) were plated in 6-well plates and grown for 24 h. After treatment, cells were collected with trypsin-EDTA, washed with PBS, and lysed with lysis buffer [150 mM NaCl, 1% Igepal-CA630, 50 mM Tris-HCl (pH 8), aprotinin (2 µg/ml), leupeptin (5 µg/ml), and 1 mM PMSF]. For PARP detection, after treatment with JB, medium and cells were collected with trypsin-EDTA and pellets were obtained by centrifugation. Cells were lysed with Laemmli sample buffer. Protein concentration was estimated by Micro BCA™ protein assay kit. Equal amounts of proteins (20 µg) were loaded and separated on a 12% polyacrylamide gel and transferred onto a PVDF membrane. Membranes were blocked in 5% milk in TBS-T 0.1% and incubated with anti-LC3, anti-p62, or anti-PARP antibody. Alternatively, membranes were

blocked with 3% BSA in TBS-T 0.1% and incubated with anti-β-actin antibody. After washing with TBS-T 0.1%, membranes were probed with the correspondent secondary antibody and protein detection was carried out using ECL and scanning the membrane with LI-COR C-DiGit® blot scanner. Band intensity was quantified by LI-COR Image Studio Lite software.

Uptake of fluid-phase tracer LY

Cells were plated at 10^5 cells/ml in 35 mm glass-bottom dishes and grown overnight. Medium was replaced with 1 ml of fresh medium containing LY (0.5 mg/ml) and cells were incubated with JB (5 μM) or ethanol (0.1%) for 16 h at 37°C, 5% CO_2. Lysotracker (75 nM) was added to each well and cells were incubated for 1 h more at 37°C, 5% CO_2. Medium was removed, cells were washed three times with PBS, and fresh DMEM FluoroBrite was added. Fluorescent images of live cells were taken using a Leica TCS-SP2 laser scanning confocal microscope, in collaboration with Scientific and Technological Centers, University of Barcelona, and the images were analyzed using Fiji-ImageJ software.

RESULTS

Synthesis

JB and *epi*-JB were synthesized from phytosphingosine stereoisomers, as previously reported (14). The corresponding *N*-octanoyl-JB (C_8-JB) and *N*-hexadecanoyl-JB (C_{16}-JB) were obtained by phosphine-catalyzed Staudinger ligation from 4-azido-JB (N_3-JB) and the corresponding carboxylic acids (supplemental Fig. S1).

JB is cytotoxic in several cell lines

We determined the cytotoxicity of JB and its derivatives in HGC-27 gastric cancer cells. JB decreased cell viability with a LD_{50} of 7.3 ± 0.7 μM (mean ± SD). The 3-*epi* and 2,3-*epi* JB showed a similar cytotoxicity compared with JB, while 2-*epi* JB was less cytotoxic than JB (LD_{50} of 12.5 ± 0.9 μM). Treatment with C_8-JB, C_{16}-JB, and N_3-JB did not cause diminished cell viability (**Table 1**). Cell viability was also evaluated in five additional cell lines, including human breast adenocarcinoma (MDA-MB 231 and MDA-MB 468), human glioblastoma (T98 and U87), and human embryonic kidney (HEK293T) cell lines in which cell viability was also decreased with LD_{50} values of 2.1 ± 0.2 μM (MDA-MB 231), 4.5 ± 2.0 μM (T98), 3.2 ± 0.9 μM (U87), and 9.5 ± 1.2 μM

TABLE 1. Cytotoxicity of JB and analogs in HGC-27 cells

Compound	LD_{50} (μM)
JB	7.3 ± 0.7
2-*epi* JB	12.5 ± 0.9
3-*epi* JB	7.6 ± 0.8
2,3-*epi* JB	4.9 ± 0.5
C_8-JB	NT
C_{16}-JB	NT
N_3-JB	NT

The cytotoxicity of the compounds was evaluated by MTT in HGC-27 cells after 24 h incubation. LD_{50} was calculated as the mean of two experiments in triplicate ± SD. NT, not toxic for the concentrations tested (930 μM).

(Hek293T) (supplemental Fig. S2). A biphasic dose-response curve was obtained in MDA-MB 468 cells.

JB induces accumulation of sphingoid bases in HGC-27 cells

Alterations in SL metabolism induced by JB have been reported in various cancer cell lines. Specifically, JB induces the accumulation of dhCer (14) and Cer and decreases levels of SM (33). To further investigate the effects of JB on SL metabolism, SL levels were determined in HGC-27 cells. MS analysis showed a dramatic increase in dhSo after 4 and 8 h. Similarly, dihydrosphingosine1-phosphate (dhSoP), which was undetectable in control samples, accumulated after 4, 8, and 24 h of JB treatment. So and sphingosine 1-phosphate (SoP) levels also increased, although to a lower extent. At all times, dhCer increased, while dihydrosphingomyelin accumulated after 24 h incubation with JB. Small changes were observed in Cer and SM levels (**Fig. 2**).

JB inhibits CerS

The accumulation of sphingoid bases suggested that JB might inhibit CerS, and this was examined using an in vitro CerS assay (32) in HEK293T cells overexpressing various CerSs. JB significantly inhibited all CerSs (**Fig. 3A**). Of the JB stereoisomers, only 2-*epi* JB inhibited CerS6 activity (~25% inhibition) (supplemental Fig. S3). Likewise, no significant inhibition of CerS6 activity was observed using C_8-JB, C_{16}-JB, and N_3-JB, indicating that the stereochemistry of JB is important for CerS inhibition and that a free amino group is necessary, in line with the cytotoxicity of JB. On the other hand, the increased levels of dhCer after JB treatment (Fig. 2) were not due to the inhibition of dhCer desaturase activity (supplemental Fig. S4).

JB is *N*-acylated by CerS

We next examined whether JB could act as a CerS substrate and thus directly *N*-acylate JB. HEK293T cells overexpressing CerS5 were incubated with JB and ^{14}C-palmitoyl-CoA (C16-[1-^{14}C]acyl-CoA). As shown in Fig. 3B, CerS5 was found to acylate JB. FB1, a CerS inhibitor (34), inhibited the *N*-acylation of JB (*N*-acylated-JB 205.40 ± 35 pmol/min/mg compared with 107.30 ± 0.2 pmol/min/mg in the presence of FB1; n = 2) The *N*-acylation of JB was confirmed by MS/TOF analysis, which showed increasing amounts of *N*-acyl-JB with different acyl chain lengths versus time (Fig. 3C). Together, these findings demonstrate that JB is directly *N*-acylated by CerS.

JB induces cell vacuolation

We next investigated the type of cell death induced by JB. HGC-27 cells exposed to JB were characterized by the accumulation of phase-lucent cytoplasmic vacuoles, which increased in size and number in a dose-dependent manner (**Fig. 4A**). Treatment with 5 μM JB caused the formation of vacuoles that were visible after 4 h of treatment and increased in size in a time-dependent manner (data not shown). The progressive accumulation of vacuoles was followed by cell rounding and detachment. Cytoplasmic
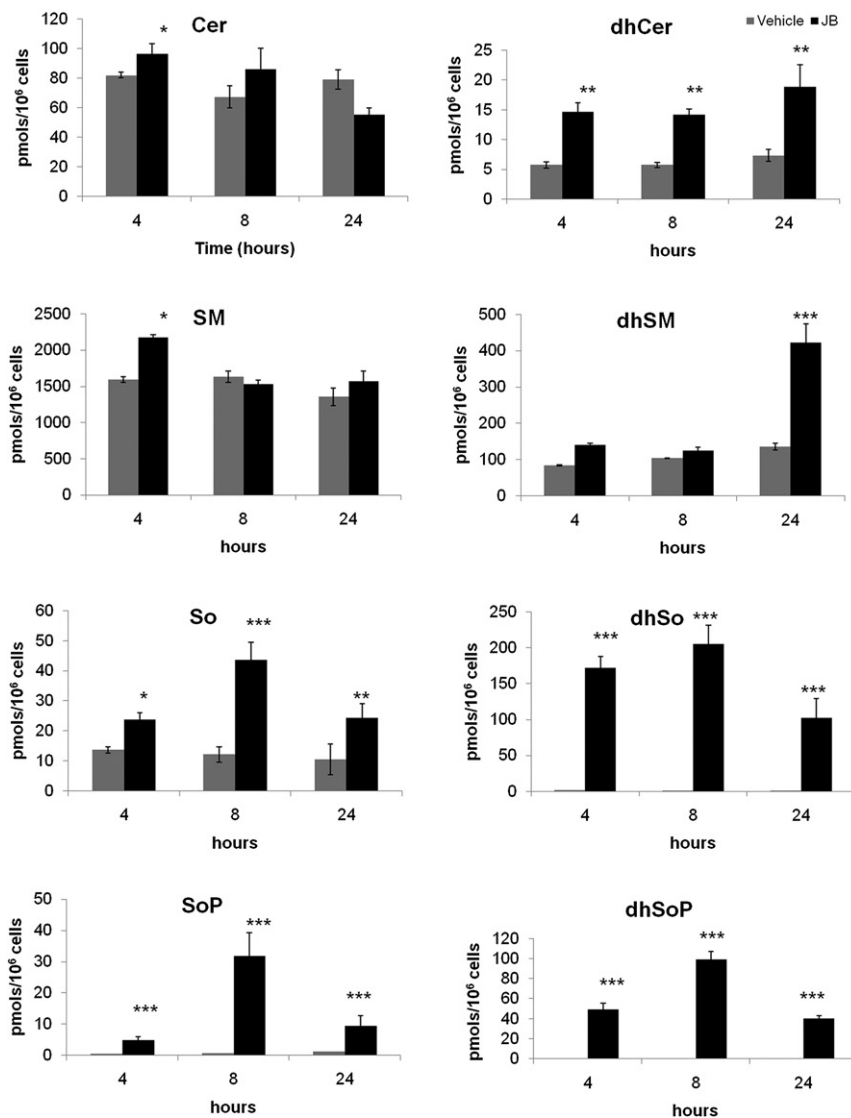
Fig. 2. Effect of JB on the HGC-27 sphingolipidome. HGC-27 cells were treated for 4, 8, and 24 h with JB (1 µM) or ethanol. Lipids were extracted and analyzed by UPLC/TOF. Triple quadrupole mass spectrometer analysis was performed to analyze So, dhSo, SoP, and dhSoP levels. $*P < 0.05$, $**P < 0.005$, $***P < 0.0005$ (n = 3).

vacuolation induced by JB was analyzed by transmission electron microscopy (TEM), which revealed that vesicles were multi-sized and formed low electron-dense areas that occupied broad cytoplasmic sections. Cellular nuclei were intact with a similar appearance to those of untreated samples (Fig. 4B). Interestingly, JB treatment of the noncancerous cell line, HEK293T, resulted in formation of vacuoles at short incubation times. However, while vacuoles persisted in the cancer cell lines examined after treatment (U87, T98, and A549 cells; supplemental Fig. S5), they were no longer present in HEK293T cells 24 h after JB administration (supplemental Fig. S6). This result suggests that JB-induced vacuolation cell death might be selective for cancer cells.

JB-induced cytotoxicity and vacuolation is not related to SL synthesis

We next investigated the effect of inhibiting SL synthesis using myriocin, an SPT inhibitor (35), on JB-induced cytotoxicity and cytoplasmic vacuolation. Myriocin caused a significant decrease in dhCer and dihydrosphingomyelin levels, which was more extensive upon JB treatment (**Fig. 5A**). Similarly, dhSo and dhSoP accumulation after JB treatment was strongly reduced when JB was combined with myriocin. Nonetheless, the decrease in dihydrosphingolipid levels induced by myriocin treatment did not affect JB cytotoxicity (Fig. 5B) or cytoplasmic vacuolation (Fig. 5C), suggesting that de novo SL synthesis and JB cytotoxicity/cytoplasmic vacuolation are independent events. In further support of this conclusion, FB1, a CerS inhibitor that also provokes increases in long-chain bases and their phosphates (34), did not induce vacuolation (supplemental Fig. S7).

Apoptosis is not involved in JB-induced vacuolation and cell death

The formation of cytoplasmic vacuoles is common to various forms of nonapoptotic cell death (36, 37). Flow cytometry analysis of annexin V/propidium iodide (PI)-stained
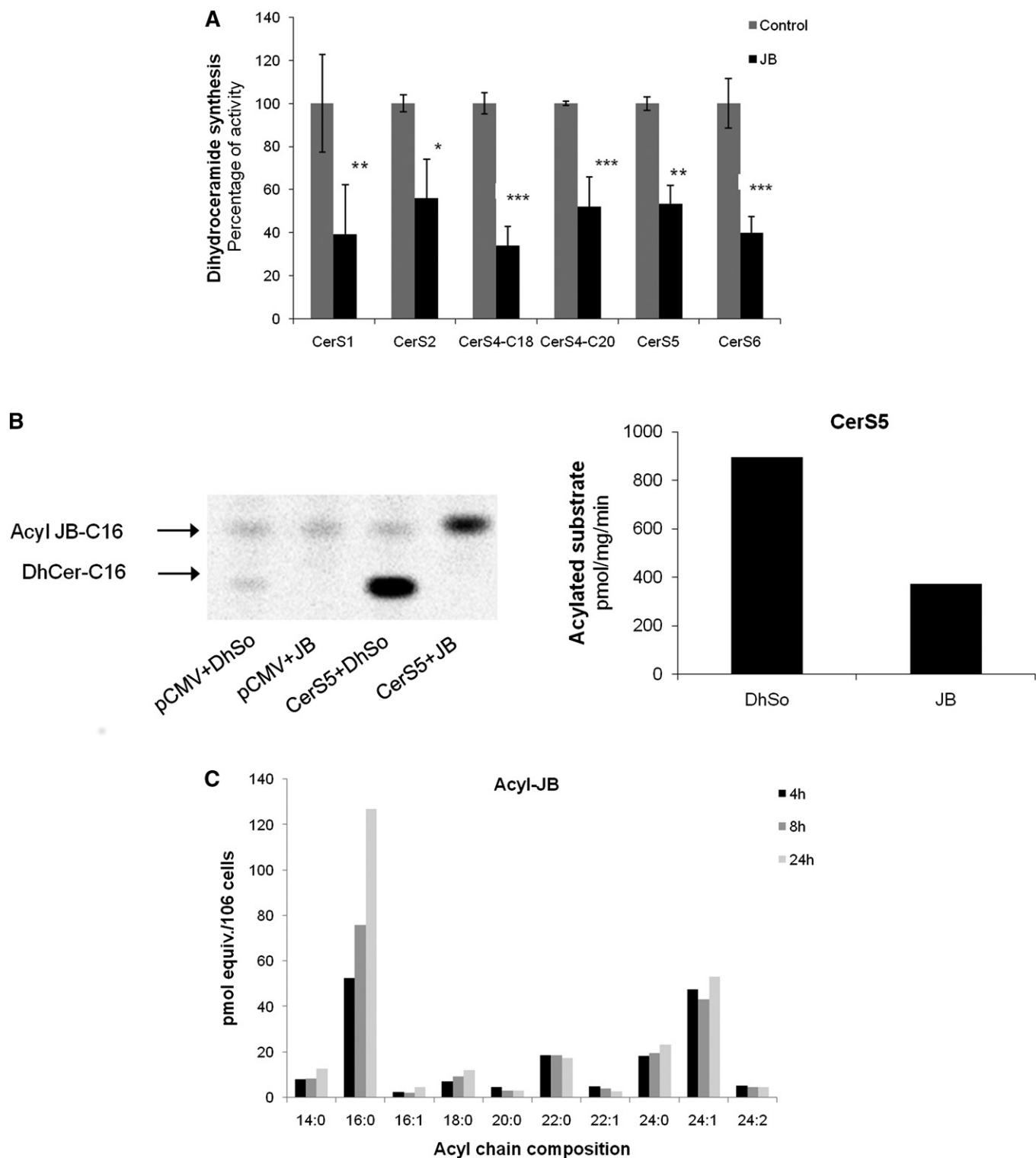
Fig. 3. JB inhibits CerS activity. A: CerS activity was determined in cell lysates overexpressing different CerSs. Lysates (CerS1, 25 μg; CerS2, 40 μg; CerS4, 30 μg; CerS5, 1 μg; CerS6, 5 μg) were preincubated for 5 min with JB (5 μM) or ethanol as a control; the reaction was started by adding NBD-dhSo (15 μM)/BSA (20 μM)/acyl-CoA (50 μM) (CerS1, C18 acyl-CoA; CerS2, C22 acyl-CoA; CerS4, C18 or C20 acyl-CoA; CerS5, C16 acyl-CoA; CerS6, acyl-CoA) to the samples. The reaction was carried out during different times (CerS1, 20 min; CerS2, 10 min; CerS4, 20 min; CerS5, 5 min; CerS6, 10 min). Results are the mean ± SD for two experiments performed in duplicate and are expressed as the percent of the activity compared with the control. *$P < 0.05$, **$P < 0.005$, ***$P < 0.0005$. B: Cell lysates overexpressing CerS5 were incubated for 20 min with DhSo or JB at 15 μM and with C16-[1-^{14}C]acyl-CoA (0.01 uCi)/C16 acyl-CoA(46 μM) and BSA (20 μM). Results are representative of a typical experiment in duplicate (n = 2). C: HGC-27 cells were treated with 1 μM JB for 4, 8, and 24 h. Lipids were extracted and analyzed by UPLC/TOF. Data are given as picomolar equivalents to C12:0 Cer and are the mean of one experiment in triplicate, which is representative of three experiments that gave similar results.
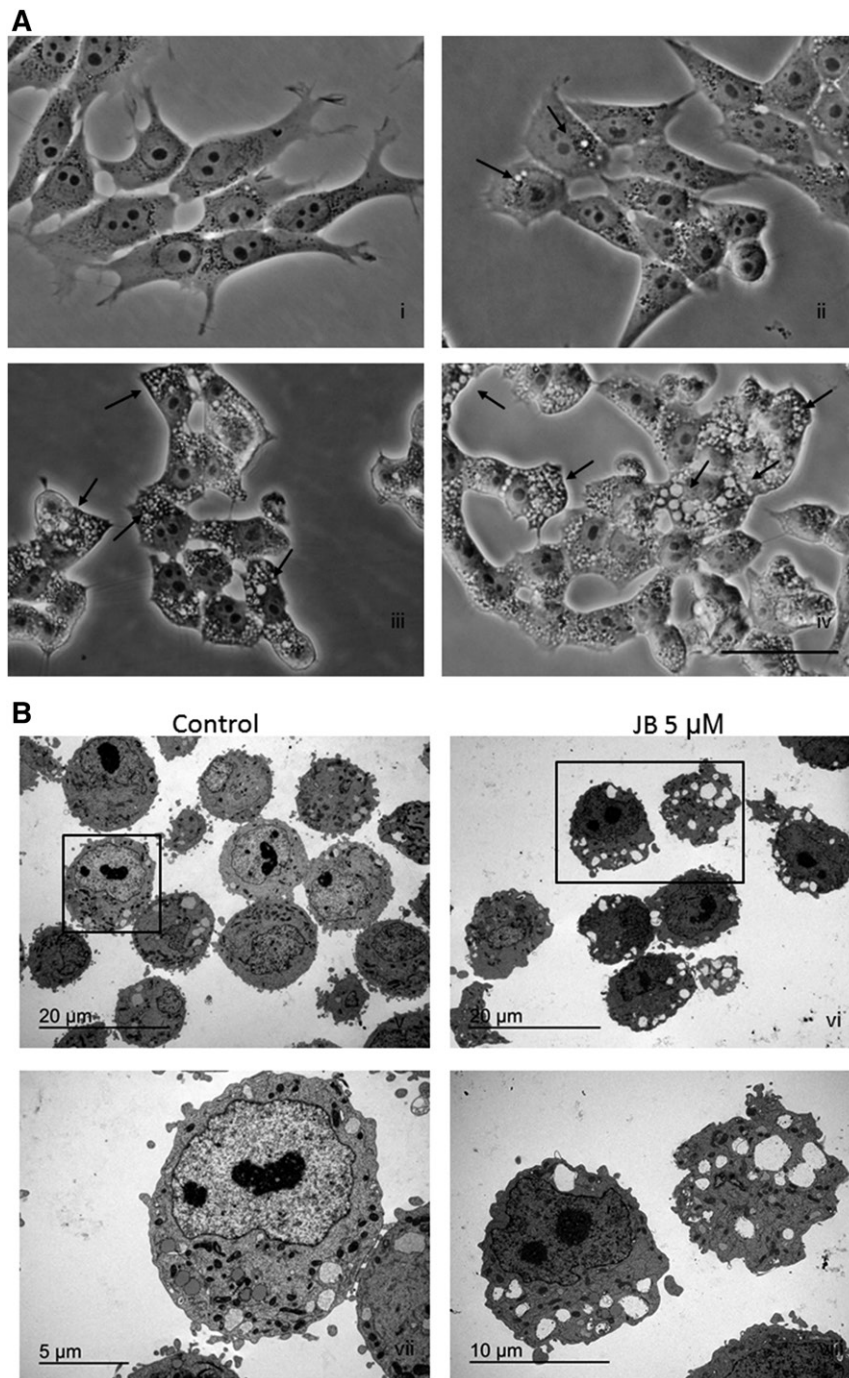
Fig. 4. JB induces cell vacuolation in HGC-27 cells. A: Phase contrast images of HGC-27 cells treated with ethanol (i) or 1 μM JB (ii), 3 μM JB (iii), or 5 μM JB (iv). Images were captured after 24 h and are representative of two experiments. Black arrows indicate cytoplasmic vesicles. Scale bar: 50 μm. B: TEM of HGC-27 cells treated with ethanol (v) or JB 5 μM (vi) for 16 h [(vii) and (viii) are higher magnifications of the selected areas of images (v) and (vi), respectively. The experiment was performed in triplicate; images are representative of the observed phenotypes.

cells demonstrated that the number of annexin V-positive cells did not increase upon treatment with 5 μM of JB. Similar results were observed when HGC-27 cells were treated with 12 μM of JB (**Fig. 6A**). Moreover, upon JB treatment, no DNA laddering or smearing (Fig. 6B), which are respectively typical of apoptosis and necrosis (38), was observed. In addition, although JB induced PARP cleavage (Fig. 6C),

this event has also been presorted to occur in nonapoptotic types of death, such as methuosis (see Discussion). Furthermore, JB cytotoxicity was evaluated in the presence of the pancaspase inhibitor, z-VAD, which did not affect JB cytotoxicity (Fig. 6D) or cytoplasmic vacuolation (Fig. 6E), demonstrating that caspase activity is not essential for JB cytotoxicity. In addition, the RIP1 kinase inhibitor, necrostatin-1, did
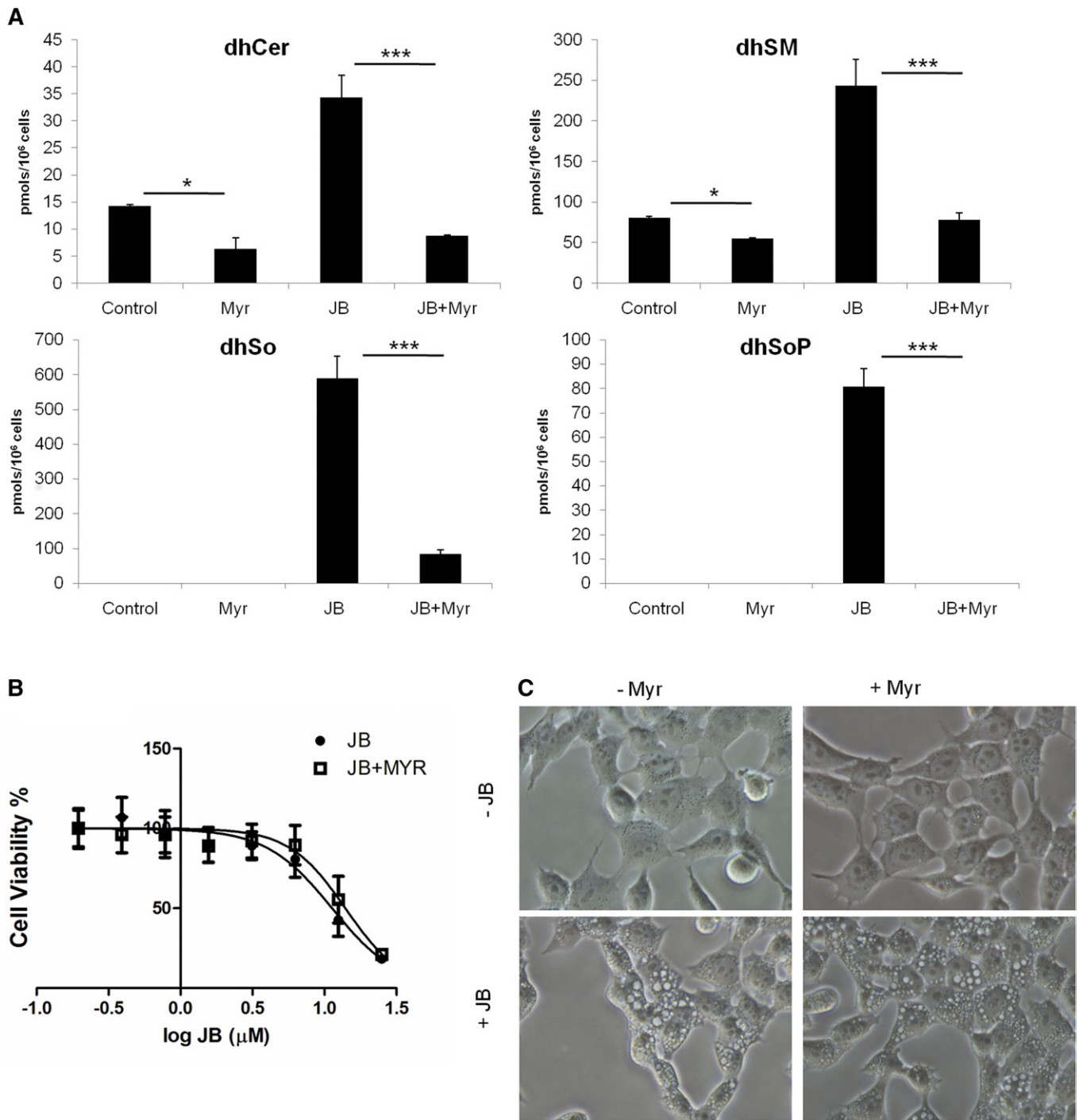
Fig. 5. Myriocin blocks de novo SL synthesis without altering JB-induced cytotoxicity and cell vacuolation. HGC-27 cells were cultured with 5 μM myriocin (Myr) or ethanol for 2 h and then incubated with 5 μM JB for 16 h. A: SLs were analyzed by UPLC-TOF MS and HPLC MS/ MS. *$P < 0.05$, ***$P < 0.0005$ (n = 3). B: HGC-27 cells were treated with 5 μM of Myr (or ethanol) for 2 h and then incubated with different concentrations of JB for 16 h. Cell viability was determined by MTT. Results are the mean ± SD of two experiments in triplicate. C: Phase contrast images are representative of the phenotype observed in two independent experiments in triplicate. Scale bar: 50 μm.

not improve cell viability (data not shown) (39, 40). Together, these findings suggest that neither apoptosis nor necrosis is involved in JB-induced cell death and vacuolation.

JB-induced vacuoles are not autophagosomes

To determine whether the vacuoles observed after JB treatment were autophagosomes or autophagolysosomes,

we measured LC3-II levels. Increased levels of LC3-II were seen in JB-treated samples, which were enhanced by preincubation with protease inhibitors (**Fig. 7A**), while treatment with the autophagy inhibitor, wortmannin, did not decrease LC3-II levels (Fig. 7B), consistent with the lack of change in levels of p62, a ubiquitin-binding scaffold protein that is degraded during autophagy (41) (Fig. 7B), and
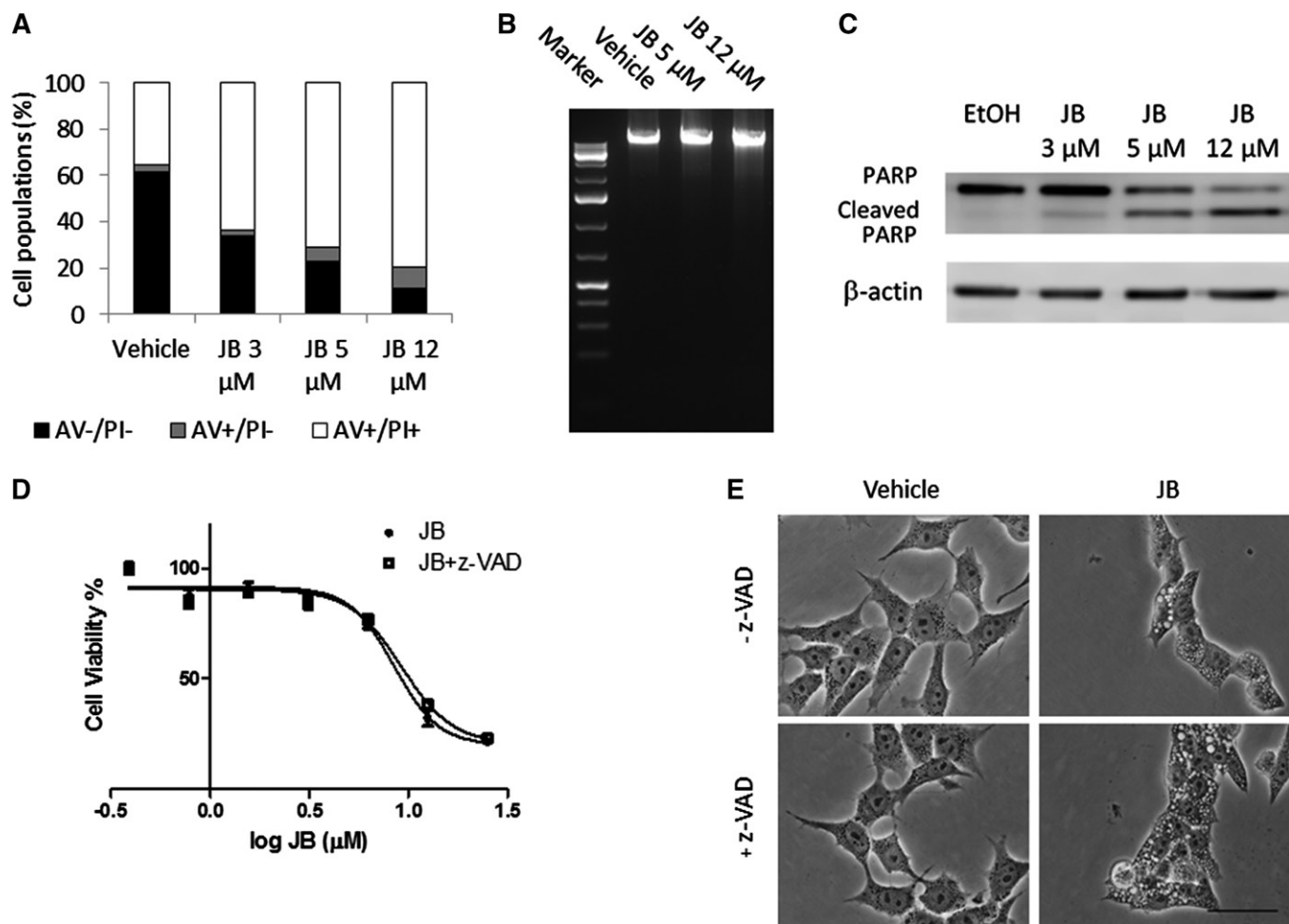
Fig. 6. JB induces nonapoptotic cell vacuolation in gastric cancer cells. A: Cells were incubated for 16 h with increasing concentrations of JB or ethanol and stained with annexin V (AV)/PI and fluorescence was analyzed by flow cytometry. The percentage of cell populations stained with AV, PI, or both are shown. Results are representative of a typical experiment in triplicate that gave similar results (n = 3). B: HGC-27 cells were treated with JB (5 or 12 μM) or ethanol (0.12%) as a control for 16 h. After extraction, DNA was run on agarose gel containing SYBR green. One hundred kilobases of DNA standard were used as a marker. The image represents a typical experiment repeated two times that gave similar results. C: HGC-27 cells were treated with JB (3, 5, and 12 μM) or ethanol as a control for 16 h. PARP and cleaved PARP were detected by Western blot. β-Actin was used as a loading control. The results are representative of four different experiments. D: JB cytotoxicity was assessed by MTT after incubating HGC-27 cells with JB for 16 h in the absence (JB) or presence (JB + z-VAD) of the pan-caspase inhibitor, z-VAD (20 μM). The results are the mean ± SD of two independent experiments repeated in triplicate. E: Phase-contrast images of cells incubated with JB (5 μM) or ethanol for 16 h in the presence of z-VAD (20 μM) (+z-VAD) or DMSO (−z-VAD). The images are representative of the observed phenotypes (n = 2).

with EM analysis, which showed that JB-induced vacuoles were single-membrane structures (Fig. 7C) rather than the double-membrane structures that characterize autophagosomes (42). In contrast, treatment with XM462, which induces autophagy in HGC-27 cells (43), resulted in formation of vacuoles typical of autophagy (Fig. 7C). Together these data demonstrate that the cytoplasmic vacuoles induced by JB treatment are not autophagic structures.

Cell vacuolation is triggered by macropinocytosis

Macropinocytosis is a regulated form of endocytosis that mediates the nonselective uptake of solute molecules, nutrients, and antigens (44, 45). Treatment with EIPA, an inhibitor of the Na^+/H^+ exchanger that blocks macropinocytosis (46, 47), prevented JB-induced cell vacuolation (**Fig. 8A**). In addition, LY, a fluid-phase tracer that is taken up by macropinocytosis (37, 45, 48, 49), colocalized with the cytoplasmic vacuoles (Fig. 8B, yellow). Importantly, these vacuoles were different from lysosomes, as they did not colocalize with LysoTracker (Fig. 8B, red). Finally, TEM analysis of cells treated with JB displayed membrane extensions (Fig. 8C, left panel) and small vesicles in the peripheral zone of cytoplasm (Fig. 8C, right panel), suggesting that the vacuoles originated from cell engulfment and then coalesced into bigger structures, thus determining cytoplasmic disruption.

DISCUSSION

Due to their structural similarity to mammalian SLs, SLs from fungi and marine organisms have been investigated
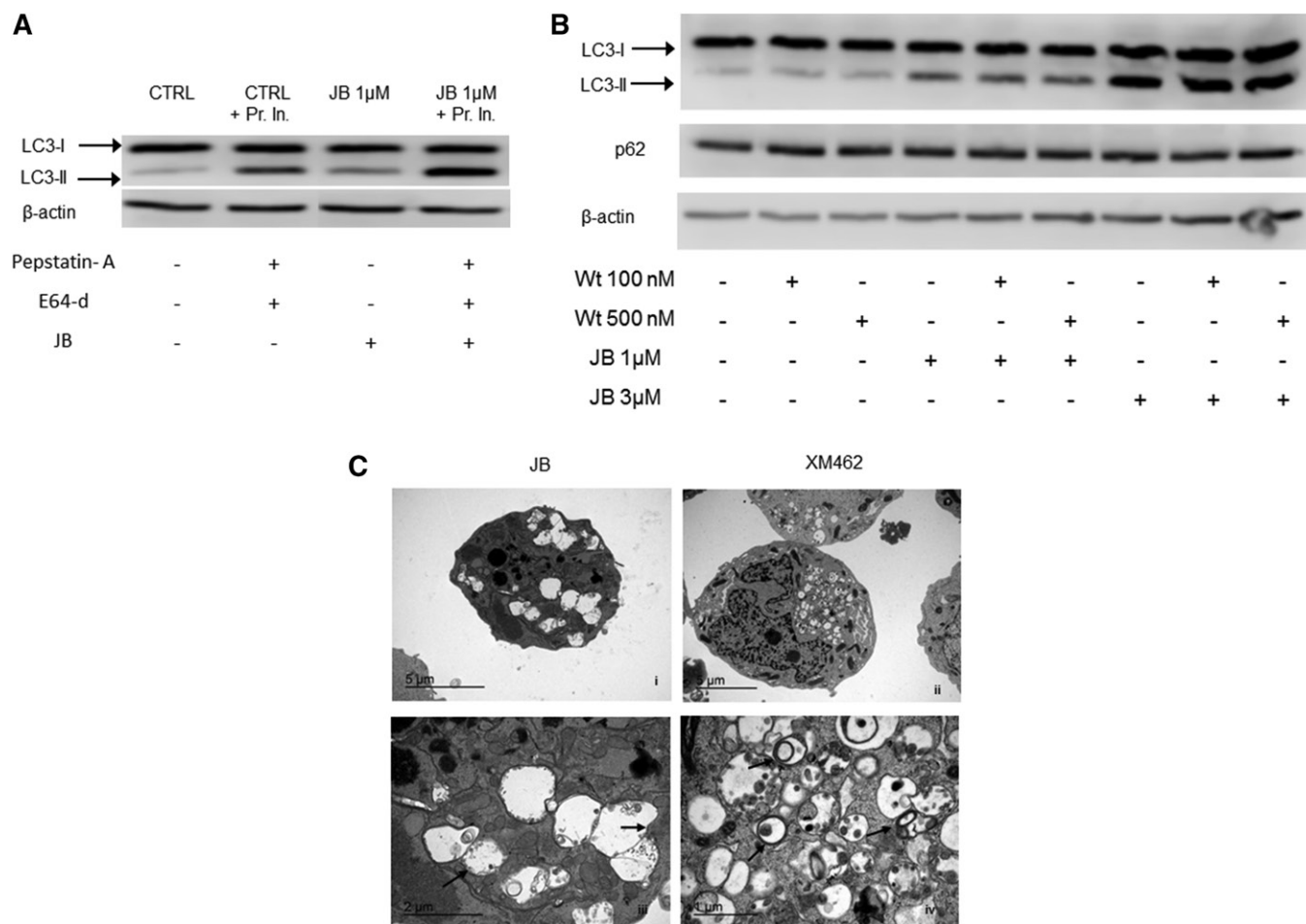
Fig. 7. JB causes autophagy-independent LC3-II accumulation. A: HGC-27 cells were treated with JB (1 μM) (or ethanol) for 16 h with or without protease inhibitors [pepstatin-A (8 μM) and E64-d (30 μM)] that were added 2 h before the treatment. B: Cells were incubated with wortmannin (Wt) (100 or 500 nM) (or DMSO) for 1 h and then with JB (1 or 3 μM) (or ethanol) for 16 h. LC3-I and LC3-II levels or p62 were detected by Western blot. β-Actin was used as a loading control. Results are representative of two to three different experiments. C: Transmission electron micrographs of HGC-27 cells treated with JB (5 μM) (i) or XM462 8 μM (ii) for 16 h. Images (iii) and (iv) represent magnifications of (i) and (ii), respectively. Arrows indicate single (ii) or double (iv) membrane vesicles. The experiment was run in triplicate; images are representative of the observed phenotypes.

as therapeutic agents for the treatment of various diseases (50). JB is a cyclic anhydrophytosphingosine from marine sponges that exhibits cytotoxic properties (11), including induction of apoptosis (13) and autophagy (14).We now have shown that JB directly interferes with SL metabolism and affects cell viability in HGC-27 gastric cancer cells.

JB inhibited CerS activity with no preference for any of the isoforms, whereas the *N*-acylated JB derivatives and the azido derivative were not inhibitory; likewise, only 2-*epi* JB inhibited CerS, although with a lower potency than JB, indicating that inhibition is stereoselective. JB was also acylated by CerS, indicating that JB likely acted as a competitive inhibitor; JB acylation resulted in a similar JB acyl chain composition as endogenous Cer generated from *N*-acylation of the natural long-chain base, dhSo. As expected, both dhSo and So levels were elevated upon incubation with JB, the former due to inhibition of de novo biosynthesis and the latter due to inhibition of the recycling/salvage pathway. This is similar to the effect of other CerS inhibitors, such as FB1 and AAL (51), both of which are structurally similar to the

sphingoid backbone. FB1 is characterized by a linear aminopentahydroxyeicosane chain in which two of the hydroxyl groups are esterified with tricarballylic acid. AAL-toxin has a similar structure, but lacks one of the tricarbal-lylic acid moieties and the terminal methyl group. JB is a sphingoid long-chain base analog that contains a terminal amino-alcohol in a heterocyclic system. The varied chemical structures of CerS inhibitors are consistent with the apparent low structural requirements of CerS toward the long-chain base. In terms of stereochemistry, the *S* configuration of C3 (bearing the secondary alcohol) is necessary for inhibition, consistent with stereochemistry of FB1, which also has an *S* configuration. All the JB stereoisomers were *N*-acylated in intact cells, although with different efficacies, as were stereoisomers of the sphingoid free bases (52), spisulosine (53, 54), FB1 (55), and HFB1 (56). Other changes in SL levels were consistent with JB action, including accumulation of dhSoP and SoP. However, the mechanism by which dhCer accumulates is not known (14), but is not due to inhibition of dhCer desaturase activity, but may
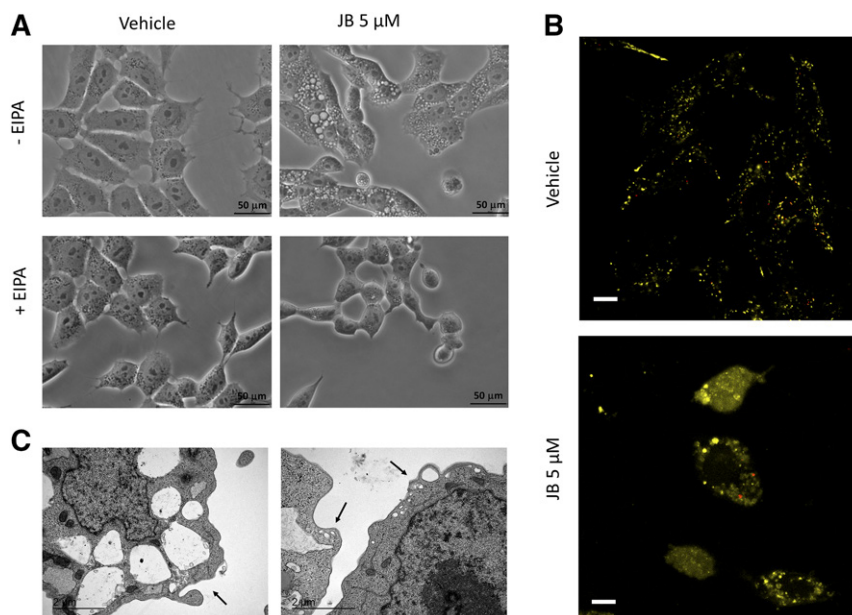
Fig. 8. Vacuoles induced by JB exhibit characteristics of macropinosomes. A: HGC-27 cells were treated with EIPA (25 μM) (or methanol) for 1 h and then JB (5 μM) (or ethanol) was added. Phase-contrast images were taken after 24 h of incubation and are representative of three independent experiments. Scale bar: 50 μM. B: Fluorescence microscopy images of HGC-27 cells after 16 h coincubation with JB (5 μM) and LY (0.5 mg/ml) and 1 h more with LysoTracker (75 nM). Images are representative of the results obtained in three independent experiments. Scale bar: 10 μM. C: Transmission electron micrographs of HGC-27 treated with JB (5 μM). After 16 h, cells were fixed and analyzed. The arrows indicate membrane extensions (left panel) and nascent macropinosomes (right panel). The experiment was run in triplicate; images are representative of the observed phenotypes.

rather be via a similar mechanism as sometimes observed upon treatment with FB1, although the latter occurs mainly when CerSs are overexpressed (57, 58).

In contrast to the cytotoxic activity of the *N*-acylated aminopentol backbone of FB1 (53), *N*-acylation of the JB amino group or conversion into an azide resulted in a noncytotoxic compound. Nevertheless, it is worth mentioning that the N-C16-derivative of JB was an acylated derivative formed from exogenous JB, while the N-C8 derivative was the acylated species exogenously administered. Although C_8-JB is transacylated to C_{16}-JB, the levels of the latter were higher from JB than from C_8-JB. This raises the possibility that C_{16}-JB is, at least in part, responsible for the observed effects of JB. On the other hand, it is also possible that the *N*-acylated JB generated from JB and the exogenously applied *N*-acylated JB target different cellular compartments and that a precise localization is necessary for the observed activity. Further experiments will be performed in the future to clarify these points. Cytotoxicity was also decreased by changing JB stereoconfiguration, consistent with the possibility that JB cytotoxicity was directly related to its effects on SL metabolism, perhaps due to changes in levels of specific SLs, which were altered upon JB treatment (59–61). Nevertheless, this was not supported by the effect of myriocin, which reduced levels of dhSo, but did not impair JB cytotoxicity. On the other hand, the effect of exogenously administered C_8-JB (the N-C16 derivative was not taken up by cells) on the sphingolipidome was negligible. Only a low marginally significant increase of So and SoP was observed,

indicating that acylated JB did not affect SL metabolism. These data support that, in case acylated JB played a role in JB-induced cell death, this effect would not be caused by alterations in natural SL levels and would strengthen the notion that the effects of JB on cell death and on SL metabolism are independent events. Thus the relationship between the changes in SL levels and the effect of JB on cytotoxicity are currently unknown.

JB promoted cell death in HGC27 cells by activating a mechanism unrelated to apoptosis, autophagy, or necrotic pathways. Although JB induced PARP cleavage, this has also been presorted to occur in nonapoptotic types of death, such as methuosis (48). Even though LC3-II levels were elevated, its levels are also elevated in some cell death mechanisms in the absence of autophagy; however, activation of autophagy as a protective mechanism in response to JB exposure cannot be entirely disregarded (30). Cell death induced by JB was characterized by dose- and time-dependent cytoplasmic vacuolation. Our data suggest that this increased vacuolation was related to hyperstimulation of macropinocytosis and was consistent with observations of lucent vacuoles in glioblastoma and lung alveolar adenocarcinoma cells exposed to JB. The presence of vesicles of different sizes and localization, some with a small dimension and localized to the external margin of the cell, and others with greater extensions and occupying a wide area in the cytoplasm, indicated that macropinosomes might coalesce into larger structures. This suggests that macropinosomes probably did not undergo maturation or recycling as

normally happens in regulated macropinocytosis (44), which might suggest altered endocytic trafficking. Likewise, upregulation and processing of LC3-II is an important event in nonautophagic cytoplasmic vacuolation and cell death, as observed upon stimulation of a nonautophagic LC3-II-dependent form of cell death in colon, breast, and prostate cancer cells by a prostaglandin, along with extensive cytoplasmic vacuolation (62), in glioblastoma (48) and prostate cancer cells (63). Finally, methamphetamine-induced macropinocytosis also causes an increase in LC3-II (64).

Cytoplasmic vacuolation is currently emerging as another type of programmed cell death. Thus, vacquinol-1 induces an endocytic-like process leading to vacuole formation, which leads to disruption of cell membrane integrity and to cell death (49); similar observations were made in gastric cancer cells and glioma cells after Ras activation. Although these vesicles were originally simply described as cytoplasmic vacuoles (65), it is now clear that the large vacuoles that accumulate in glioblastoma are enlarged macropinosomes, a process named "methuosis" (from the Greek "methuo," meaning "to drink to intoxication") (48); a similar phenomenon was observed with the chalcone derivative, 3-(5-methoxy-2-methyl-1H-indol-3-yl)-1-(4-pyridinyl)-2-propen-1-one, in glioblastoma cells (66). A number of other studies have reported a similar pathway in cancer cells, such as upon treatment of apoptosis-resistant MCL cells with WIN55,212-2, which induces paraptosis-like cell death (67), treatment with the farnesyl protease transferase inhibitor manumycin A, which reduces cancer cell viability through induction of nonapoptotic nonautophagic cytoplasmic vacuolation death in triple-negative breast cancers (68), and upon treatment with the natural polyphenolic pigment, curcumin, which induces vacuolation-related cell death in human PC-3M prostate cancer cells. Although a large number of molecules were shown to induce phenotypes similar to JB-induced vacuolation (69), a specific readout defining macropinocytic vacuole accumulation has not yet been provided. However, the involvement of Ras and Src proteins appears to be a common element in dysregulated macropinocytosis and vacuolation-induced cell death (69–72) and might represent key molecules for JB-induced vacuolation. However, at present, we do not know whether methuosis is also induced by JB, but we suggest that JB might be a useful tool to examine this novel cell death pathway. Moreover, we are unable to provide a direct mechanistic link between cytoplasmic vacuolation and cytotoxicity induced by JB and changes in SL levels. Interestingly, PF543, a SK1 inhibitor, caused decreased cell vacuolation and death (data not shown) in agreement with a report showing a connection between cell vacuolation and SK1 depletion in glioblastoma cells treated with both the SK inhibitor, SKI-II, and temozolomide (28), concomitant with accumulation of dhSo and dhCer. However, the fact that FB1 did not induce cell vacuolation despite increasing the levels of long-chain bases and their phosphates is against a role of these lipids in vacuolation cell death.

In summary, we suggest that JB joins the growing list of compounds that induce cytoplasmic vacuolation and methuosis (49, 64, 66, 67, 73–76) and we suggest that JB might be a novel way to interrogate this emerging pathway, which appears to be selective for cancer cell lines.■

REFERENCES

1. Futerman, A. H., and Y. A. Hannun. 2004. The complex life of simple sphingolipids. *EMBO Rep.* **5:** 777–782.

2. Gault, C. R., L. M. Obeid, and Y. A. Hannun. 2010. An overview of sphingolipid metabolism: from synthesis to breakdown. *Adv. Exp. Med. Biol.* **688:** 1–23.

3. Gangoiti, P., L. Camacho, L. Arana, A. Ouro, M. H. Granado, L. Brizuela, J. Casas, G. Fabriás, J. L. Abad, A. Delgado, and A. Gómez-Muñoz. 2010. Control of metabolism and signaling of simple bioactive sphingolipids: implications in disease. *Prog. Lipid Res.* **49:** 316–334.

4. Sandhoff, K. 2013. Metabolic and cellular bases of sphingolipidoses. *Biochem. Soc. Trans.* **41:** 1562–1568.

5. Delgado, A., G. Fabrias, C. Bedia, J. Casas, and J. L. Abad. 2012. Sphingolipid modulation: a strategy for cancer therapy. *Anticancer. Agents Med. Chem.* **12:** 285–302.

6. Maceyka, M., and S. Spiegel. 2014. Sphingolipid metabolites in inflammatory disease. *Nature.* **510:** 58–67.

7. van Echten-Deckert, G., and J. Walter. 2012. Sphingolipids: critical players in Alzheimer's disease. *Prog. Lipid Res.* **51:** 378–393.

8. Sabourdy, F., L. Astudillo, C. Colacios, P. Dubot, M. Mrad, B. Ségui, N. Andrieu-Abadie, and T. Levade. 2015. Monogenic neurological disorders of sphingolipid metabolism. *Biochim. Biophys. Acta.* **1851:** 1040–1051.

9. Hannich, J. T., K. Umebayashi, and H. Riezman. 2011. Distribution and functions of sterols and sphingolipids. *Cold Spring Harb. Perspect. Biol.* **3:** a004762.

10. Delgado, A., J. Casas, A. Llebaria, J. L. Abad, and G. Fabriás. 2007. Chemical tools to investigate sphingolipid metabolism and functions. *ChemMedChem.* **2:** 580–606.

11. Kuroda, I., M. Musman, I. I. Ohtani, T. Ichiba, J. Tanaka, D. G. Gravalos, and T. Higa. 2002. Pachastrissamine, a cytotoxic anhydrophytosphingosine from a marine sponge, Pachastrissa sp. *J. Nat. Prod.* **65:** 1505–1506.

12. Ledroit, V., C. Debitus, C. Lavaud, and G. Massiot. 2003. Jaspines A and B: two new cytotoxic sphingosine derivatives from the marine sponge Jaspis sp. *Tetrahedron Lett.* **44:** 225–228.

13. Salma, Y., E. Lafont, N. Therville, S. Carpentier, M-J. Bonnafé, T. Levade, Y. Génisson, and N. Andrieu-Abadie. 2009. The natural marine anhydrophytosphingosine, Jaspine B, induces apoptosis in melanoma cells by interfering with ceramide metabolism. *Biochem. Pharmacol.* **78:** 477–485.

14. Canals, D., D. Mormeneo, G. Fabriàs, A. Llebaria, J. Casas, and A. Delgado. 2009. Synthesis and biological properties of Pachastrissamine (jaspine B) and diastereoisomeric jaspines. *Bioorg. Med. Chem.* **17:** 235–241.

15. Yoshimitsu, Y., J. Miyagaki, S. Oishi, N. Fujii, and H. Ohno. 2013. Synthesis of pachastrissamine (jaspine B) and its derivatives by the late-stage introduction of the C-2 alkyl side-chains using olefin cross metathesis. *Tetrahedron.* **69:** 4211–4220.

16. Shelke, A. M., V. Rawat, A. Sudalai, and G. Suryavanshi. 2014. A short enantioselective synthesis of 3-epi-jaspine B and (+)-oxybiotin via an intramolecular tandem desilylation oxa-Michael addition strategy. *RSC Adv.* **4:** 49770–49774.

17. Xu, J. M., E. Zhang, X. J. Shi, Y. C. Wang, B. Yu, W. W. Jiao, Y. Z. Gou, and H. M. Liu. 2014. Synthesis and preliminary biological evaluation of 1,2,3-triazole-jaspine B hybrids as potential cytotoxic agents. *Eur. J. Med. Chem.* **80:** 593–604.

18. Kwon, Y., J. Song, H. Bae, W. J. Kim, J-Y. Lee, G. H. Han, S. K. Lee, and S. Kim. 2015. Synthesis and biological evaluation of carbocyclic analogues of pachastrissamine. *Mar. Drugs.* **13:** 824–837.

19. Rives, A., S. Ladeira, T. Levade, N. Andrieu-Abadie, and Y. Génisson. 2010. Synthesis of cytotoxic aza analogues of jaspine B. *J. Org. Chem.* **75:** 7920–7923.

20. Yoshimitsu, Y., S. Oishi, J. Miyagaki, S. Inuki, H. Ohno, and N. Fujii. 2011. Pachastrissamine (jaspine B) and its stereoisomers inhibit sphingosine kinases and atypical protein kinase C. *Bioorg. Med. Chem.* **19:** 5402–5408.

21. Cingolani, F., A. H. Futerman, and J. Casas. 2016. Ceramide synthases in biomedical research. *Chem. Phys. Lipids.* **197:** 25–32.

22. Lahiri, S., H. Lee, J. Mesicek, Z. Fuks, A. Haimovitz-Friedman, R. N. Kolesnick, and A. H. Futerman. 2007. Kinetic characterization of mammalian ceramide synthases: determination of K(m) values towards sphinganine. *FEBS Lett.* **581:** 5289–5294.

23. Saddoughi, S. A., P. Song, and B. Ogretmen. 2008. Roles of bioactive sphingolipids in cancer biology and therapeutics. *Subcell. Biochem.* **49:** 413–440.

24. Lépine, S., B. Lakatos, P. Maziere, M-P. Courageot, J-C. Sulpice, and F. Giraud. 2002. Involvement of sphingosine in dexamethasone-induced thymocyte apoptosis. *Ann. N. Y. Acad. Sci.* **973:** 190–193.

25. Cuvillier, O., V. E. Nava, S. K. Murthy, L. C. Edsall, T. Levade, S. Milstien, and S. Spiegel. 2001. Sphingosine generation, cytochrome c release, and activation of caspase-7 in doxorubicin-induced apoptosis of MCF7 breast adenocarcinoma cells. *Cell Death Differ.* **8:** 162–171.

26. Ahn, E. H., and J. J. Schroeder. 2002. Sphingoid bases and ceramide induce apoptosis in HT-29 and HCT-116 human colon cancer cells. *Exp. Biol. Med. (Maywood).* **227:** 345–353.

27. Ahn, E. H., C-C. Chang, and J. J. Schroeder. 2006. Evaluation of sphinganine and sphingosine as human breast cancer chemotherapeutic and chemopreventive agents. *Exp. Biol. Med. (Maywood).* **231:** 1664–1672.

28. Noack, J., J. Choi, K. Richter, A. Kopp-Schneider, and A. Régnier-Vigouroux. 2014. A sphingosine kinase inhibitor combined with temozolomide induces glioblastoma cell death through accumulation of dihydrosphingosine and dihydroceramide, endoplasmic reticulum stress and autophagy. *Cell Death Dis.* **5:** e1425.

29. Separovic, D., J. Bielawski, J. S. Pierce, S. Merchant, A. L. Tarca, B. Ogretmen, and M. Korbelik. 2009. Increased tumour dihydroceramide production after Photofrin-PDT alone and improved tumour response after the combination with the ceramide analogue LCL29. Evidence from mouse squamous cell carcinomas. *Br. J. Cancer.* **100:** 626–632.

30. Signorelli, P., J. M. Munoz-Olaya, V. Gagliostro, J. Casas, R. Ghidoni, and G. Fabriàs. 2009. Dihydroceramide intracellular increase in response to resveratrol treatment mediates autophagy in gastric cancer cells. *Cancer Lett.* **282:** 238–243.

31. Bedia, C., J. Casas, N. Andrieu-Abadie, G. Fabriàs, and T. Levade. 2011. Acid ceramidase expression modulates the sensitivity of A375 melanoma cells to dacarbazine. *J. Biol. Chem.* **286:** 28200–28209.

32. Tidhar, R., K. Sims, E. Rosenfeld-Gur, W. Shaw, and A. H. Futerman. 2015. A rapid ceramide synthase activity using NBD-sphinganine and solid phase extraction. *J. Lipid Res.* **56:** 193–199.

33. Salma, Y., S. Ballereau, S. Ladeira, C. Lepetit, R. Chauvin, N. Andrieu-Abadie, and Y. Genisson. 2011. Single- and double-chained truncated jaspine B analogues: asymmetric synthesis, biological evaluation and theoretical study of an unexpected 5-endo-dig process. *Tetrahedron.* **67:** 4253–4262.

34. Merrill, A. H., D. C. Liotta, and R. T. Riley. 1996. Fumonisins: fungal toxins that shed light on sphingolipid function. *Trends Cell Biol.* **6:** 218–223.

35. Wadsworth, J. M., D. J. Clarke, S. A. McMahon, J. P. Lowther, A. E. Beattie, P. R. R. Langridge-Smith, H. B. Broughton, T. M. Dunn, J. H. Naismith, and D. J. Campopiano. 2013. The chemical basis of serine palmitoyltransferase inhibition by myriocin. *J. Am. Chem. Soc.* **135:** 14276–14285.

36. Kornienko, A., V. Mathieu, S. K. Rastogi, F. Lefranc, and R. Kiss. 2013. Therapeutic agents triggering nonapoptotic cancer cell death. *J. Med. Chem.* **56:** 4823–4839.

37. Maltese, W. A., and J. H. Overmeyer. 2014. Methuosis: nonapoptotic cell death associated with vacuolization of macropinosome and endosome compartments. *Am. J. Pathol.* **184:** 1630–1642.

38. Collins, J. A., C. A. Schandl, K. K. Young, J. Vesely, and M. C. Willingham. 1997. Major DNA fragmentation is a late event in apoptosis. *J. Histochem. Cytochem.* **45:** 923–934.

39. Degterev, A., Z. Huang, M. Boyce, Y. Li, P. Jagtap, N. Mizushima, G. D. Cuny, T. J. Mitchison, M. A. Moskowitz, and J. Yuan. 2005. Chemical inhibitor of nonapoptotic cell death with therapeutic potential for ischemic brain injury. *Nat. Chem. Biol.* **1:** 112–119.

40. Galluzzi, L., I. Vitale, J. M. Abrams, E. S. Alnemri, E. H. Baehrecke, M. V. Blagosklonny, T. M. Dawson, V. L. Dawson, W. S. El-Deiry, S. Fulda, et al. 2012. Molecular definitions of cell death subroutines: recommendations of the Nomenclature Committee on Cell Death 2012. *Cell Death Differ.* **19:** 107–120.

41. Bjørkøy, G., T. Lamark, S. Pankiv, A. Øvervatn, A. Brech, and T. Johansen. 2009. Monitoring autophagic degradation of p62/SQSTM1. *Methods Enzymol.* **452:** 181–197.

42. Tooze, S. A., and T. Yoshimori. 2010. The origin of the autophagosomal membrane. *Nat. Cell Biol.* **12:** 831–835.

43. Gagliostro, V., J. Casas, A. Caretti, J. L. Abad, L. Tagliavacca, R. Ghidoni, G. Fabrias, and P. Signorelli. 2012. Dihydroceramide delays cell cycle G1/S transition via activation of ER stress and induction of autophagy. *Int. J. Biochem. Cell Biol.* **44:** 2135–2143.

44. Lim, J. P., and P. A. Gleeson. 2011. Macropinocytosis: an endocytic pathway for internalising large gulps. *Immunol. Cell Biol.* **89:** 836–843.

45. Kerr, M. C., and R. D. Teasdale. 2009. Defining macropinocytosis. *Traffic.* **10:** 364–371.

46. West, M. A., M. S. Bretscher, and C. Watts. 1989. Distinct endocytotic pathways in epidermal growth factor-stimulated human carcinoma A431 cells. *J. Cell Biol.* **109:** 2731–2739.

47. Koivusalo, M., C. Welch, H. Hayashi, C. C. Scott, M. Kim, T. Alexander, N. Touret, K. M. Hahn, and S. Grinstein. 2010. Amiloride inhibits macropinocytosis by lowering submembranous pH and preventing Rac1 and Cdc42 signaling. *J. Cell Biol.* **188:** 547–563.

48. Overmeyer, J. H., A. Kaul, E. E. Johnson, and W. A. Maltese. 2008. Active ras triggers death in glioblastoma cells through hyperstimulation of macropinocytosis. *Mol. Cancer Res.* **6:** 965–977.

49. Kitambi, S. S., E. M. Toledo, D. Usoskin, S. Wee, A. Harisankar, R. Svensson, K. Sigmundsson, C. Kalderén, M. Niklasson, S. Kundu, et al. 2014. Vulnerability of glioblastoma cells to catastrophic vacuolization and death induced by a small molecule. *Cell.* **157:** 313–328.

50. Delgado, A., G. Fabriàs, J. Casas, and J. L. Abad. 2013. Natural products as platforms for the design of sphingolipid-related anticancer agents. *Adv. Cancer Res.* **117:** 237–281.

51. Abbas, H. K., T. Tanaka, S. O. Duke, J. K. Porter, E. M. Wray, L. Hodges, A. E. Sessions, E. Wang, A. H. Merrill, Jr., and R. T. Riley. 1994. Fumonisin- and AAL-toxin-induced disruption of sphingolipid metabolism with accumulation of free sphingoid bases. *Plant Physiol.* **106:** 1085–1093.

52. Venkataraman, K., and A. H. Futerman. 2001. Comparison of the metabolism of L-erythro- and L-threo-sphinganines and ceramides in cultured cells and in subcellular fractions. *Biochim. Biophys. Acta.* **1530:** 219–226.

53. Humpf, H. U., E. M. Schmelz, F. I. Meredith, H. Vesper, T. R. Vales, E. Wang, D. S. Menaldino, D. C. Liotta, and A. H. Merrill, Jr. 1998. Acylation of naturally occurring and synthetic 1-deoxysphinganines by ceramide synthase. Formation of N-palmitoyl-aminopentol produces a toxic metabolite of hydrolyzed fumonisin, AP1, and a new category of ceramide synthase inhibitor. *J. Biol. Chem.* **273:** 19060–19064.

54. Abad, J. L., I. Nieves, P. Rayo, J. Casas, G. Fabriàs, and A. Delgado. 2013. Straightforward access to spisulosine and 4,5-dehydrospisulosine stereoisomers: probes for profiling ceramide synthase activities in intact cells. *J. Org. Chem.* **78:** 5858–5866.

55. Harrer, H., E. L. Laviad, H. U. Humpf, and A. H. Futerman. 2013. Identification of N-acyl-fumonisin B1 as new cytotoxic metabolites of fumonisin mycotoxins. *Mol. Nutr. Food Res.* **57:** 516–522.

56. Seiferlein, M., H. U. Humpf, K. A. Voss, M. C. Sullards, J. C. Allegood, E. Wang, and A. H. Merrill, Jr. 2007. Hydrolyzed fumonisins HFB1 and HFB2 are acylated in vitro and in vivo by ceramide synthase to form cytotoxic N-acyl-metabolites. *Mol. Nutr. Food Res.* **51:** 1120–1130.

57. Lahiri, S., H. Park, E. L. Laviad, X. Lu, R. Bittman, and A. H. Futerman. 2009. Ceramide synthesis is modulated by the sphingosine analog FTY720 via a mixture of uncompetitive an noncompetitive inhibition in a Acyl-CoA chain length-dependent manner. *J. Biol. Chem.* **284:** 16090–16098.

58. Venkataraman, K., C. Riebeling, J. Bodennec, H. Riezman, J. C. Allegood, M. C. Sullards, A. H. Merrill, Jr., and A. H. Futerman. 2002. Upstream of growth and differentiation factor 1 (uog1), a mammalian homolog of the yeast longevity assurance gene 1 (LAG1), regulates N-stearoyl-sphinganine (C18-(dihydro)ceramide) synthesis in a fumonisin B1-independent manner in mammalian cells. *J. Biol. Chem.* **277:** 35642–35649.

59. Tolleson, W. H., L. H. Couch, W. B. Melchior, G. R. Jenkins, M. Muskhelishvili, L. Muskhelishvili, L. J. McGarrity, O. Domon, S. M. Morris, and P. C. Howard. 1999. Fumonisin B1 induces apoptosis in

cultured human keratinocytes through sphinganine accumulation and ceramide depletion. *Int. J. Oncol.* **14:** 833–843.

60. Mao, Z., W. Sun, R. Xu, S. Novgorodov, Z. M. Szulc, J. Bielawski, J. M. Obeid, and C. Mao. 2010. Alkaline ceramidase 2 (ACER2) and its product dihydrosphingosine mediate the cytotoxicity of N-(4-hydroxyphenyl)retinamide in tumor cells. *J. Biol. Chem.* **285:** 29078–29090.

61. Jiang, Q., X. Rao, C. Y. Kim, H. Freiser, Q. Zhang, Z. Jiang, and G. Li. 2012. Gamma-tocotrienol induces apoptosis and autophagy in prostate cancer cells by increasing intracellular dihydrosphingosine and dihydroceramide. *Int. J. Cancer.* **130:** 685–693.

62. Kar, R., P. K. Singha, M. A. Venkatachalam, and P. Saikumar. 2009. A novel role for MAP1 LC3 in nonautophagic cytoplasmic vacuolation death of cancer cells. *Oncogene.* **28:** 2556–2568.

63. Florey, O., S. E. Kim, C. P. Sandoval, C. M. Haynes, and M. Overholtzer. 2011. Autophagy machinery mediates macroendocytic processing and entotic cell death by targeting single membranes. *Nat. Cell Biol.* **13:** 1335–1343.

64. Nara, A., T. Aki, T. Funakoshi, and K. Uemura. 2010. Methamphetamine induces macropinocytosis in differentiated SH-SY5Y human neuroblastoma cells. *Brain Res.* **1352:** 1–10.

65. Chi, S., C. Kitanaka, K. Noguchi, T. Mochizuki, Y. Nagashima, M. Shirouzu, H. Fujita, M. Yoshida, W. Chen, A. Asai, et al. 1999. Oncogenic Ras triggers cell suicide through the activation of a caspase-independent cell death program in human cancer cells. *Oncogene.* **18:** 2281–2290.

66. Trabbic, C. J., H. M. Dietsch, E.M. Alexander, P. I. Nagy, M. W. Robinson, J. H. Overmeyer, W. A. Maltese, and P. W. Erhardt. 2014. Differential induction of cytoplasmic vacuolization and methuosis by novel 2-indolyl-substituted pyridinylpropenones. *ACS Med. Chem. Lett.* **5:** 73–77.

67. Wasik, A. M., S. Almestrand, X. Wang, K. Hultenby, A-L. Dackland, P. Andersson, E. Kimby, B. Christensson, and B. Sander. 2011. WIN55,212–2 induces cytoplasmic vacuolation in apoptosis-resistant MCL cells. *Cell Death Dis.* **2:** e225.

68. Arenz, C., M. Thutewohl, O. Block, H. Waldmann, H. J. Altenbach, and A. Giannis. 2001. Manumycin A and its analogues are irreversible inhibitors of neutral sphingomyelinase. *ChemBioChem.* **2:** 141–143.

69. Shubin, A. V., I. V. Demidyuk, A. A. Komissarov, L. M. Rafieva, and S. V. Kostrov. 2016. Cytoplasmic vacuolization in cell death and survival. *Oncotarget.* **7:** 55863–55889.

70. Li, C., J. I. MacDonald, A. Talebian, J. Leuenberger, C. Seah, S. H. Pasternak, S. W. Michnick, and S. O. Meakin. 2016. Unravelling the mechanism of TrkA-induced cell death by macropinocytosis in medulloblastoma Daoy cells. *Mol. Cell. Biol.* **36:** 2596–2611.

71. Park, J. K., H. Peng, J. Katsnelson, W. Yang, N. Kaplan, Y. Dong, J. Z. Rappoport, C. He, and R. M. Lavker. 2016. MicroRNAs-103/107 coordinately regulate macropinocytosis and autophagy. *J. Cell Biol.* **215:** 667–685.

72. Manara, M. C., M. Terracciano, C. Mancarella, M. Sciandra, C. Guerzoni, M. Pasello, A. Grilli, N. Zini, P. Picci, M. P. Colombo, et al. 2016. CD99 triggering induces methuosis of Ewing sarcoma cells through IGF-1R/RAS/Rac1 signaling. *Oncotarget.* **7:** 79925–79942.

73. Robinson, M. W., J. H. Overmeyer, A. M. Young, P. W. Erhardt, and W. A. Maltese. 2012. Synthesis and evaluation of indole-based chalcones as inducers of methuosis, a novel type of nonapoptotic cell death. *J. Med. Chem.* **55:** 1940–1956.

74. Singha, P. K., S. Pandeswara, M. A. Venkatachalam, and P. Saikumar. 2013. Manumycin A inhibits triple-negative breast cancer growth through LC3-mediated cytoplasmic vacuolation death. *Cell Death Dis.* **4:** e457.

75. Lee, W. J., M. H. Chien, J. M. Chow, J. L. Chang, Y. C. Wen, Y. W. Lin, C. W. Cheng, G. M. Lai, M. Hsiao, and L. M. Lee. 2015. Nonautophagic cytoplasmic vacuolation death induction in human PC-3M prostate cancer by curcumin through reactive oxygen species -mediated endoplasmic reticulum stress. *Sci. Rep.* **5:** 10420.

76. Isobe, I., Y. Maeno, M. Nagao, M. Iwasa, H. Koyama, Y. Seko-Nakamura, and J. Monma-Ohtaki. 2003. Cytoplasmic vacuolation in cultured rat astrocytes induced by an organophosphorus agent requires extracellular signal-regulated kinase activation. *Toxicol. Appl. Pharmacol.* **193:** 383–392.